



Subscriber access provided by Texas A&M University Libraries

Article

3D Printing Super Strong Hydrogel for Artificial Meniscus

Zimeng Zhang, Ruochen Liu, Herman Zepeda, Li Zeng, Jingjing Qiu, and Shiren Wang

ACS Appl. Polym. Mater., Just Accepted Manuscript • DOI: 10.1021/acsapm.9b00304 • Publication Date (Web): 01 Jul 2019

Downloaded from http://pubs.acs.org on July 6, 2019

Just Accepted

"Just Accepted" manuscripts have been peer-reviewed and accepted for publication. They are posted online prior to technical editing, formatting for publication and author proofing. The American Chemical Society provides "Just Accepted" as a service to the research community to expedite the dissemination of scientific material as soon as possible after acceptance. "Just Accepted" manuscripts appear in full in PDF format accompanied by an HTML abstract. "Just Accepted" manuscripts have been fully peer reviewed, but should not be considered the official version of record. They are citable by the Digital Object Identifier (DOI®). "Just Accepted" is an optional service offered to authors. Therefore, the "Just Accepted" Web site may not include all articles that will be published in the journal. After a manuscript is technically edited and formatted, it will be removed from the "Just Accepted" Web site and published as an ASAP article. Note that technical editing may introduce minor changes to the manuscript text and/or graphics which could affect content, and all legal disclaimers and ethical guidelines that apply to the journal pertain. ACS cannot be held responsible for errors or consequences arising from the use of information contained in these "Just Accepted" manuscripts.

3D Printing Super Strong Hydrogel for Artificial Meniscus

Zimeng Zhang^{a,1}, Ruochen Liu^{b, 1}, Herman Zepeda^a, Li Zeng^a, Jingjing Qiu^c, Shiren Wang^{a,b*}

- ^a Department of Industrial and Systems Engineering, Texas A&M University, College Station, TX 77843, USA
- ^b Department of Materials Science and Engineering, Texas A&M University, College Station, TX 77843, USA
- ^c Department of Mechanical Engineering, Texas Tech University, Lubbock, TX 77409, USA
- *Corresponding Author Email: s.wang@tamu.edu
- ¹ These authors have equal contributions

Abstract

3D printing of artificial meniscus affords the great potential to overcome the supply shortage of transplantation; however, the inferior mechanical properties post as a huge roadblock for this potential. This paper demonstrates 3D printing of super-strong hydrogel for eliminating this barrier. Specifically, a multiple-ingredient ink consisting of cellulose nanocrystal (CNC), hard phenyl acrylate (PA), and soft acrylamide (AAm) components were developed to print super strong hydrogel toward artificial meniscus application. The effect of cellulose nanocrystal fraction on the printability of the complex ink was investigated and found >8% cellulose nanocrystal is required for adjusting the ink viscosity and thus making the ink to be printable. As-printed inks were crosslinked to form interpenetrated polymer network via UV irradiation, resulting in numerous randomly-distributed hard PA-rich regions and soft AAm-rich regions in the an interpenetrated gel network. The synergistic effect of hard and soft phases on mechanical performance was studied. Hydrogels printed with a PA/AAm ratio of 4:2 an exhibited exceptional tensile strength of ~16.5 MPa but poor toughness ~1.8 MJ m⁻³ due to too high PA

molar ratio. The hydrogel with a PA/AAm ratio of 3:2 demonstrates a tensile strength of ~4.4 MP and toughness of ~6 MJ m⁻³, which are equivalent to or even superior to the performance of human meniscus. Finally, printing of such hydrogel-based artificial meniscus was demonstrated and the printing precision was studied.

Key Words: 3D printing, hydrogel, rheological behavior, mechanical performance, artificial meniscus

1. Introduction

The meniscus is a wedge-shaped piece of fibrocartilaginous tissue which acts as a "cushion" between the shinbone and thighbone in the knee joint¹⁻⁸. It is reported that about 1.5 million people need meniscus treatments in the US and Europe every year^{3, 6-7, 9}. Oftentimes meniscus deficiency will lead to advanced osteoarthritis (OA) due to wound lesions if timely treatment is not received. A slight meniscal tear can be healed by the injection of functional biomaterials, suturing or partial meniscus replacement, while severe injuries often require meniscus transplantation. However, limitations lie in donor supply, shape mismatch, and tissue compatibility. As a promising solution, the fabrication of an artificial meniscus is highly demanded.

Challenges of engineering an artificial meniscus include mimicking the complex structure of meniscus with individualized features and superior mechanical performance required to mimic the natural meniscus (e.g., high compressive strength, tensile strength, toughness, shock absorption and low friction). Emerging 3D printing technology can construct the freeform structure by the addition of successive layers of materials which offers high geometric fidelity, structure complexity, and design flexibility. Therefore, it allows patient-specific meniscus fabriaction¹⁰⁻¹¹. Among them, the mechanical performance of 3D printed an artificial meniscus

highly depends on the material properties¹². Seeking suitable materials to achieve the mechanical performance of natural meniscus is a real challenge. Though endeavors of synthesizing different hydrogels by varying proportions of ingredients were reported, the resultant mechanical performance is still far inferior to the natural tissues and not able to meet the demand¹². Another concern is the biological response to the selected material, which in turn directed the biocompatibility. The understanding of biocompatibility is critical in determining tissue longevity and functionality.

Hydrogels consisting of crosslinked macromolecules and water is a class of biomaterials prevalent in today's load-bearing tissue fabrication¹³⁻¹⁴. To date, four types of hydrogels have been fabricated via mold processing, including nanocomposites (NC) gel¹⁵⁻¹⁷, ionic-covalent entanglement (ICE) gel¹⁸⁻¹⁹, slide-ring (SR) gel²⁰⁻²¹ and double network (DN) gel²²⁻²⁴. Among them, DN gels attracted extensive attention for their excellent mechanical performance. The exceptional properties observed on DN gels were attributed to the synergistic effect of interpenetrated hard and soft polymer networks via an energy dissipation mechanism. The most attractive DN gels are poly(2-acrylamido,2-methyl,1-propanesulfonic acid) (PAMPS)/PAAm, alginate/PAAm²⁴, agar/PAAm²², etc., which demonstrated mechanical performance superior to their individual components. Especially, the PAMPS/PAAm DN gel fabricated by molding process demonstrated tensile strength ranging from 1 to 10 MPa, compressive strength of 20-60 MPa and toughness of 10³-10⁴ kJ m⁻³, which are superior to other types of hydrogels and comparable to the natural meniscus^{23, 25}. Such exceptional properties were accredited to a primary rigid and brittle network interoperated with a secondary soft and ductile network and well-controlled crosslinking density (tightly crosslinked first network and loosely crosslinked second network)²⁶.

Although molded hydrogels could achieve high mechanical properties, the molding process is difficult to produce the precise geometry features of the meniscus. Lack of geometry precision will lead to mismatch and many transplantation problems of the meniscus. Emerging 3D printing can readily produce the high-fidelity meniscus, but it is difficult to create desired interpenetrated network in a layer-by-layer deposition manner. Many attempts have been devoted to preparing printable inks with suitable viscosity, viscoelasticity and instant sol-gel transition for printing^{27, 28, 29}. Yang et al. reported a suitable printing viscosity ranging from 10³ to 10⁴ Pa s to store the ink in the cartridge and avoid high extrusion pressure²⁸. To achieve instant sol-gel transition, both ion responsive and temperature responsive 18 polymer were incorporated. In addition, the introduction of high aspect ratio nanostructures (nanosilicates) induced shear thinning behavior and formed secondary electrostatic crosslinking with charged polymer chains to improve the viscoelastic properties¹⁸. Chimene et al. incorporated gelatin methacryloyl (GelMA) and nanosilicates to functionalize their bioinks with temperature responsive sol-gel transition and improved shear thinning and viscoelasticity¹⁸. Recently, the PAMPS/PAAm DN hydrogel was printed via a two-step method where the second PAAm network was formed after the first PAMPS network was printed and crosslinked²⁸. The resulting DN gel showed a tensile strength of 1.4 MPa²⁸. Later, Li et al. reported a dual ionic crosslinking method for printing alginate/poly(acrylamide-co-acrylic acid)/Fe³⁺ DN gel. The printed DN gel exhibited higher strength of 3.24 MPa³⁰. However, the mechanical performance of 3D printed hydrogel is still inferior to the molding-processed hydrogel, and not able to meet the transplantation demand.

In this work, we incorporate 3D printing to fabricate a strong artificial meniscus using a novel hydrogel ink which contains both soft (AAm) and hard (phenyl acrylate(PA)) components with different hydrophilic and hydrophobic properties and can be crosslinked in one step forming

the P(PA-co-AAm) copolymer. PA is chosen to introduce the hydrophobic region in the copolymer chain to improve mechanical performance due to the presence of hard benzene groups. The synthesized copolymer exhibited superior mechanical strength and toughness also attributed to the synergistic effect of hard (hydrophobic) and soft (hydrophilic) components. Cellulose nanocrystals (CNCs) were introduced to tune the viscosity for enhancing the printability of the ink. The mechanical properties of printed hydrogel were then studied.

2. Materials and Methods

2.1 Materials

The phenyl acrylate (PA) was purchased from Tokyo Chemical Industry Co., Ltd. Acrylamide (AAm), N,N'-methylenebisacrylamide (MBAA), and Irgacure 2959 (2-Hydroxy-4'-(2-hydroxyethoxy)-2-methylpropiophenone) were purchased from Sigma Aldrich. Dimethyl sulfoxide (DMSO) was purchased from Micro Fine Chemicals. Cellulose nanocrystal (CNC) was kindly provided by CelluForce Inc.

2.2 Preparation of inks

The hydrogel precursor was prepared by dissolving 1.0 g of CNC and 50 mg Irgacure 2959 in 8.1 g of DMSO. The solution was homogenized via stirring and bubbled nitrogen gas bubbled. A series of inks with a certain initial molar concentration of PA and AAm was prepared and slowly added. The inks were labeled by molar concentration of components, denoted as PA:AAm_(x:y:z) and copolymer hydrogels formed by the corresponding ink were denoted as P(PA-co-AAm)_(x:y:z) (where x, y and z represent the molar concentration of PA, AAm and MBAA, respectively).

2.3 3D printing of super strong hydrogel

To print the gel, structures were first designed in Solidworks and converted to G-code using Slic3r software. The commercial 3D bioprinter (Allevi 1) was used to print the copolymer hydrogel where prepared ink was loaded in the cartridge and extruded out via pneumatic force. The extrusion pressure varies according to the different ink formulations. The 24-gauge needles were used for printing at a speed of 2 mm/s under a pressure range of 5-10 psi. After printing, the part was crosslinked under UV irradiation (Spectroline, ENF-280C) at a wavelength of 365nm in a nitrogen atmosphere for 10 min. Fourier-transform infrared spectroscopy (FTIR, Bruker, ALPHA-PLatinum) was employed for chemical structure characterization. The dimension of parts was measured using a caliper before and after placing the parts in deionized (DI) water for solvent exchange. Using the same printing parameters, a meniscus-like construct was printed using PA:AAm_(3:2:0.05) hydrogel precursor.

2.4 Morphological and rheological characterization

Scanning electron microscopy (JEOL JSM-7500F) was applied to characterize the micromorphology of printed hydrogels. The sample was frozen and freeze-dried before SEM characterization.

A rheometer (Anton Paar Physica MCR-301) was used for testing the rheological behavior of hydrogel precursor. Viscosities of prepared solutions with varied CNC concentrations were measured by a 50 mm CP50-1 plate geometry.

2.5 Solvent content

The DMSO content (Q_1) and water content (Q_2) after solvent exchange were measured, and the weights of as-printed (W_i) , solvent-exchanged (W_a) , placed in air (for 1 hour) (W'_a) , and freeze-dried hydrogel (W_d) were measured and calculated by the following formulae:

$$Q_1 = \frac{W_i - W_d}{W_d} \times 100\%$$
 (1)

$$6 (2)$$

$$Q_2 = \frac{W_a - W_d}{W_d} \times 100\%$$

Water content of hydrogel specimens after (Q'_2) 1-hour exposure in air after solvent exchange was calculated by

$$Q_2' = \frac{W_a' - W_d}{W_d} \times 100\% \tag{3}$$

2.6 Mechanical characterization

Dogbone samples were printed with a modified dimension of ASME VSM-5 standard model for tensile testing on an Instron 3345 tensile test machine (Instron Corporation, MA, USA) with a maximum load of 2 kN. The cross-section area of the dogbone samples was measured by caliper before testing and sandpaper was used to prevent slipping during measurement. The tensile testing speed was set to 10 mm min⁻¹. The measurement was carried out at room temperature (\sim 25 °C). The Young's modulus was calculated using the stress-strain curve with a strain from 0 to 10%. The gel toughness (Γ_c) was obtained by calculating the area under the stress-strain curve.

Cylinder with 10 mm diameter and 3 mm height was prepared for compression test using the same Instron test machine with a maximum load of 10 kN. The speed was set to 5 mm min⁻¹ for a single cycle compression test. The exact size of the parts was measured before testing. Dynamic compression test with 25 cycles with maximum compression strain of 40% was also analyzed. The speed was set to 1 mm min⁻¹. All the specimens were tested directly after printing or after solvent exchange.

2.7 Statistical Analysis

The quantitative experimental results were studied and presented as mean \pm standard deviation. One-way analysis of variance (ANOVA) and pairwise comparison (Bonferroni

method) were employed in the statistical analysis. We use *, ** and *** to indicate the statistical significance with p < 0.1, p < 0.005, and p < 0.0005, respectively.

3. Results and Discussion

Single network hydrogels of copolymer chains were 3D printed and crosslinked via a facile reaction. The hydrogel was designed based on the idea of incorporating both the hard (hydrophobic) and soft (hydrophilic) polymer chains in one network. Because PA is insoluble in water, the hydrogel precursor was first prepared in an organic solvent (DMSO) followed by a solvent exchange process to obtain the hydrogel. The fabrication of the proposed gel is illustrated in Figure 1a. The hydrogel precursor is a mixture of PA (forming hard region with the presence of benzene ring), AAm (forming soft region with superior elasticity) and crosslinker. In accommodation to the printing process, CNCs were also incorporated for tuning the viscosity of the ink. The presence of photoinitiators (Irgacure 2959) initiated the crosslinking reaction under UV irradiation (365 nm) and then transformed liquid to gel. After crosslinking, the copolymer chains (chemical structures are shown in Figure 1a below the organogel) extended when surrounded by organic solvents. In this condition, grafted benzene side groups on the copolymer chains were well dispersed in the solvent and the benzene groups were separated by the amide groups to prevent π - π aromatic interactions. The copolymer chains with both hydrophilic amide side groups, dispersed benzene groups and the corresponding molecular structure was shown in Figure 1a (i). When water diffused into the gel, benzene groups had a tendency to expel water and aggregate together forming a densely packed 3D hard region with lower water content. A bendable hard gel was formed after the solvent exchange. The molecular structure of the hard region and the aromatic interactions between two benzene groups were shown in Figure 1a (ii). Due to the one-pot synthesis, the hard region and soft region were randomly distributed in the

copolymer. Figure 1b shows the 3D bioprinter printing the proposed ink precursor. Figures 1c and 1d are photos of as-printed organogel and the hydrogel obtained after soaking in DI water for 1 hour, respectively. The color changed from clear transparent to opaque white after the solvent exchange. FTIR was employed to analyze the gel formation and SEM was applied to characterize the microstructure, shown in Figure S1 and Figure S2, respectively. The missing peak at 1560 and 1570 cm⁻¹ indicates the successful crosslinking of PA and AAm. The SEM image of P(PA-co-AAm)_(3:2) hydrogel shows a densely compacted microstructure with small-scale 0.5-1.5 µm micropores.

Compared to previous 3D printed hydrogels, the single network copolymer exhibited superior performance with the simplified printing process. Characterization and analysis of its printability, mechanical performance and water content are given in the following subsections.

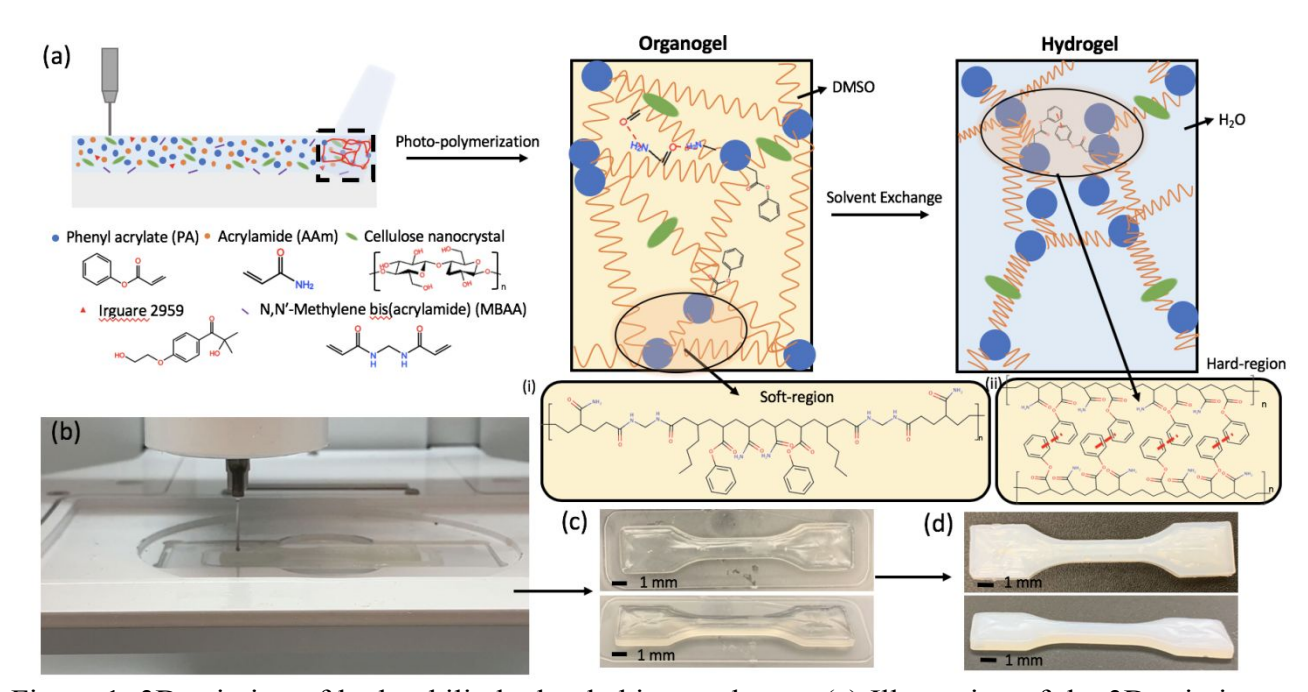


Figure 1. 3D printing of hydrophilic-hydrophobic copolymer. (a) Illustration of the 3D printing process and structure transformation after solvent exchange; (b) Image of the 3D printing process;

(c) Image of as-printed dogbone specimen; (d) Image of dogbone specimen after solvent exchange.

3.1 Extrusion based 3D printing

The 3D printable single network consisting of both hard and soft phases was inspired by the P(PA-co-AAm) hydrogel discovered by Jeon et al³¹. To make the hydrogel precursor printable, CNCs were added as the rheological modifier to improve the viscosity and maintain the shape after printing. In addition, the shear thinning behavior was also induced from high aspect ratio CNC³²⁻³⁵. CNC is a biocompatible material derived from natural woods with crystallized structure. It has been widely studied in various biomedical applications as filler or main component for enhanced mechanical performance³⁶.

Viscosity (η) of the CNC/DMSO solution with different concentrations was measured to determine the suitable printing range. The measurement results are displayed in Figure 2a and the viscosity-shear rate curves for each CNC concentration showed in Figure S3. The curve exhibited shear thinning behavior where the ink viscosity dramatically decreased with the increasing shear rate during printing and the high shear force suddenly disappeared and reverted to high viscosity at low shear rate. The viscosity-shear rate curves follow a power law model³⁷:

$$\eta = K\dot{\gamma}^{n-1} \tag{4}$$

Here, $\dot{\gamma}$ is the testing shear rate, K is the consistency index, and n is the power law index. K represents the value of apparent viscosity of the fluid at a shear rate of 1 s⁻¹, and n indicates the degree of shear thinning behavior. As the CNC concentration increased to 8 wt%, the solution exhibited shear thinning behavior (n<1). As the CNC concentration continued to increase, the shear thinning behavior became more significant (n increased), and much thicker (K increased), as shown in Table S1. The calculation of n and K were explained in supporting material and

shown in Figure S4. Higher CNC concentration (12wt%) was selected for more significant shear thinning behavior and sufficient viscosity that required to avoid sagging and spreading¹⁹. The viscosity behavior with the addition of PA and AAm monomer was also characterized. The shear thinning behavior of the PA: AAm_(3:2)/12 wt% CNC solution was also observed, shown in Figure 2b. The shear rates of the ink endured in the cartridge and needle were calculated using the equation below³⁸:

$$\dot{\gamma} = \frac{8\nu}{d} \tag{5}$$

Here, v is the linear fluid flow rate (printing speed) and d is the inside diameter of the cartridge or needle. The printing speed is set to 2 mm s⁻¹ in this work. The inside diameter of the cartridge and needle are 16 mm and 0.311 mm, respectively. So, the calculated shear rates in both conditions are 1 s⁻¹ (in the cartridge) and 51 s⁻¹ (in the needle), corresponding to the viscosities of 100 Pa·s and 1.1 Pa·s in Figure 2b. After depositing the material on the platform, the shear rate approaching 0 resulting in the dramatic increase in viscosity¹⁸. Compared to a previous report²⁸, the viscosity of the ink is lower, but still printable because the required viscosity for printing varies upon needle gauge, printing speed and capability of the printer (adjustable pressure range). As mentioned in section 2.3, 24-gauge needles were used for printing under pressure ranges in 5-

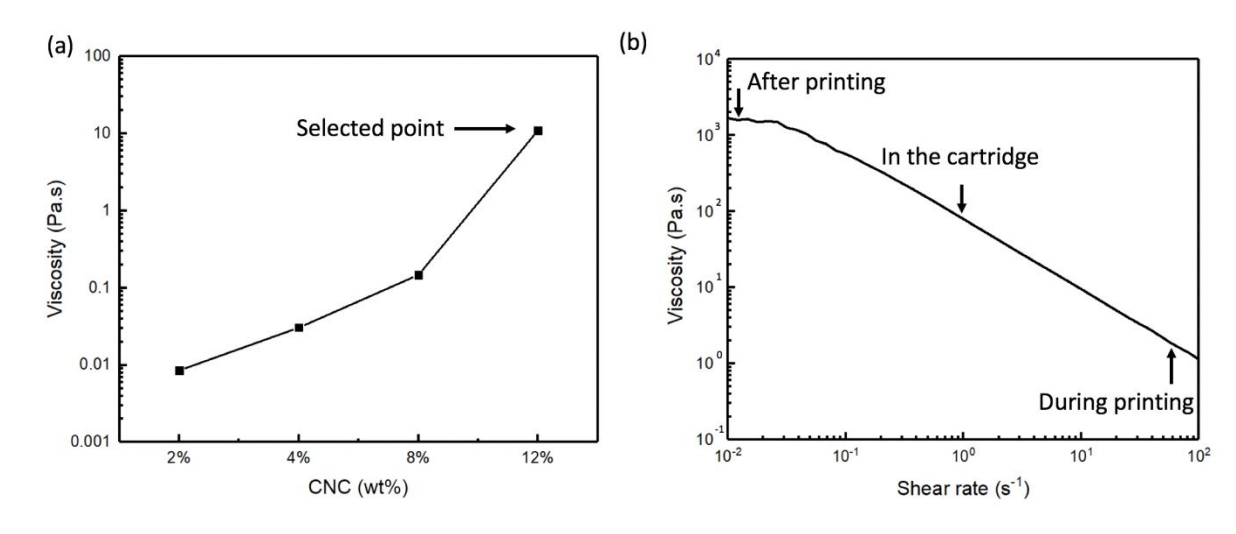


Figure 2. Rheology measurement. (a) The viscosity of aqueous solutions with different CNC concentrations at a constant shear rate of 10 s⁻¹; (b) Viscosity of the 3D printable solution as a function of shear rate.

3.2 Tensile characterization

The prospects of the printed PA:AAm hydrogels in load bearing applications were evaluated in tension first. Dogbone shaped specimen was printed for tensile testing, shown in Figures 3a, 3b, and 3c. The typical stress-strain curves of printed hydrogels with various PA:AAm compositions are illustrated in Figure 3d. P(PA-co-AAm)_(4:2) presented a superior strength (~19 MPa) but limited strain (~20%) compared to other compositions due to the high concentration of PA. For other compositions, extended strain up to 180% was observed while the strength was less than 5 MPa. This was due to the higher molar ratio of elastic AAm group in the copolymer chain. Besides, comparable tensile strength was observed for molded and printed hydrogels where the organogel demonstrated a significantly lower strength (~0.5 MPa) at the same material concentration. This indicates the effective tensile strength enhancement of P(PAco-AAm) gel after solvent exchange. The enhancement in tensile strength may contribute to the aggregation of hydrophobic benzene groups which expelled the surrounding water molecules and formed a hard region in the hydrogel. Furthermore, unlike conventional printing process where the tensile performance of 3D printed specimens deteriorates due to the lack of interlayer bonding, the involvement of solvent exchange helps reduce the interfacial gap. The reduction in the height of the printed specimens further proved the reduction in the interfacial gap, as shown in Table S2.

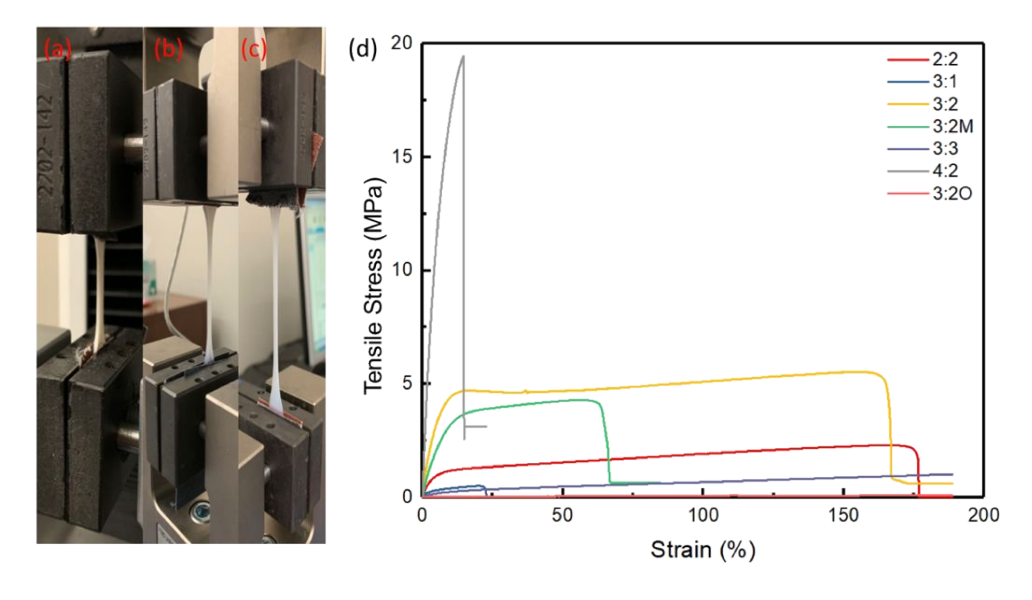


Figure 3. Tensile characterization. (a) Tensile experiment of P(PA-co-AAm)_(4:2) hydrogel; (b), (c) Tensile experiment of P(PA-co-AAm)_(3:2) hydrogel. (d) Tensile stress-strain curve.

The tensile strength, Young's modulus and toughness of the hydrogels with a series of PA:AAm molar ratios are shown in Figure 4. At least three specimens were prepared for each hydrogel composition. Figures 4a demonstrate the effect of PA monomer concentration on the tensile performance. The inset picture in Figure 4a shows hydrogel specimens of different PA:AAm molar ratios (2:2, 3:2, 4:2, 3:1, 3:3 from left to right). With the increasing PA concentration, the hydrogel was getting less transparent. When the PA:AAm molar ratio reached 4:2, the specimen became completely white and opaque. This was caused by the high concentration of hydrophobic PA and increased aggregation of the benzene groups. The tensile strength was greatly improved with the increasing PA concentration at the same AAm concentration. Young's modulus was determined by the slope of the elastic region (linear potion) of the stress-strain curve, while toughness was calculated by the area under the curve. Tensile strength, Young's modulus and toughness were ~4.4 MPa, ~40.6 MPa, and ~5.9 MJ m⁻³ at P(PA-

co-AAm)_(3:2) molar concentrations and changed to ~16.7 MPa, ~232.4 MPa, and 1.5 MJ m⁻³ at the higher PA molar concentration of P(PA-co-AAm)_(4:2). The decrease of toughness can be explained by the higher PA molar ratio which resulted in the significant reduction of fracture strain. Thus, the PA concentration was fixed at 3 mol% and the suitable AAm concentration was then determined. Similarly, the tensile strength, Young's modulus and toughness of hydrogels with fixed PA concentration but different AAm concentrations were analyzed. Toughness of printed hydrogels with different PA:AAm molar ratios are shown in Figure 4b. For specimens of P(PA-co-AAm)_(3:1), the tensile strength, Young's modulus and toughness all reached their summit, which are ~0.4 MPa, ~ 9.7 MPa, and ~0.1 MJ m⁻³, respectively, much inferior to the P(PA-co-AAm)_(3:2) hydrogels. Further increase of AAm concentration above 2 mol% led to the reduction of tensile performance. These results indicated that the copolymer exhibits the optimal tensile performance when the elastic component and the rigid component reach their balance³¹. The statistical significance of the aforementioned measurement results shown in Figure 4 including tensile strength, modulus and toughness were indicated in Table S4-S6.

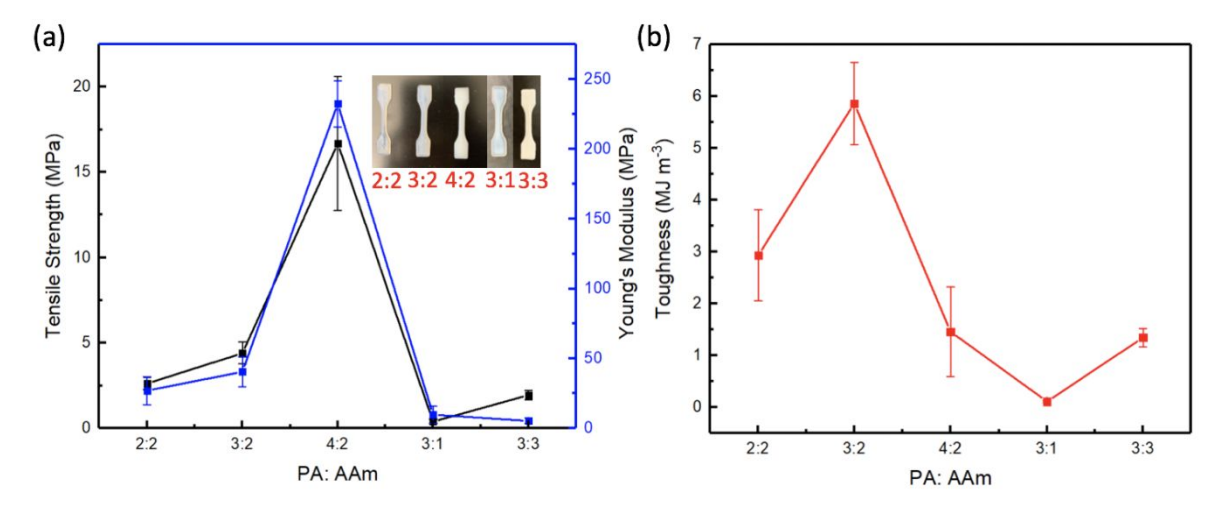


Figure 4. (a) Tensile strength, Young's modulus and (b) Toughness of printed hydrogel with varied PA and AAm concentrations.

The effect of solvent exchange time was characterized by immersing specimens in DI water for a different time period ranging from 0 to 60 minutes with an interval of 15 minutes. The stress-strain curves are given in Figure S5 and the inset picture shows the tested specimens with different immersing times. There is a significant increase in tensile stress after immersing in water for 60 minutes, but a slight decrease in fracture strain. The results also indicate that the water content of the hydrogel specimens affects the tensile performance.

To further understand the solvent effect on mechanical performance, the water content was calculated for each PA:AAm composition, shown in Figure 5. Both the water content after solvent exchange and the water content after placing the hydrogel specimens in the air for 1 hour after solvent exchange were characterized. These are represented by the weight loss ratio (Q_1, Q_2) after hydrogel was freeze dried. From the calculation results, the water content was closely related to the PA:AAm concentration. The water content greatly reduced with the increasing concentration of PA, whereas the water content increases with the increasing concentration of AAm. This can be explained by the intrinsic hydrophobicity of PA and hydrophilicity of AAm. In addition, the loss of water content is indicated by the difference between the two water content values. It is observed that higher concentration of PA is more susceptible to water loss due to the increase of PA aggregation which expelled an increased amount of water. This phenomenon is also validated by the color change during solvent exchange where higher PA concentration resulted in whiter and more opaque hydrogels, as shown in the inset image of Figure 4a.

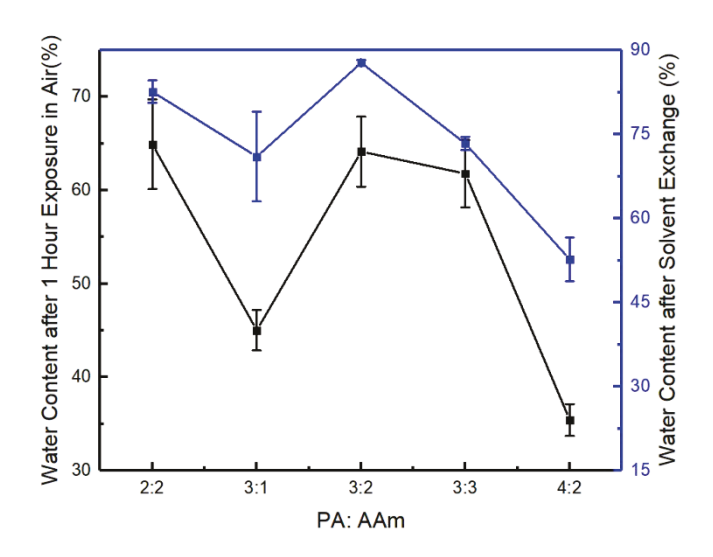


Figure 5. Water content calculation of hydrogel specimens with varying PA:AAm ratios

Specimens with high PA concentration and low AAm concentration, though exhibiting exceptional tensile strength, are hard to keep water from evaporation. They can easily drop below the water content lower bound of natural soft tissues such as skin and cartilage, specifically in the range of 50 wt% to 70 wt%39-40. Therefore, exceeding PA concentrations like 3:1, 4:2 compositions are not ideal. The composition of P(PA-co-AAm)_(3:2) which exhibited a high water content and the rate of water loss is considered more suitable for artificial meniscus fabrication. The above results further confirmed the importance of water content in determining hydrogel performance. The statistical significance of the comparison between specimens with different PA:AAm compositions presented in Figure 5 were analyzed and the results were shown in Table S7, S8.

The crosslinker effect on the tensile performance was also studied, shown in Figure 6. The image of tested specimens is given in the inset of Figure 6a. By tuning the concentration of MBAA (0.25 mol% to 0.75 mol%) while fixing PA:AAm molar ratio (3:2), no obvious difference in tensile strength was observed. The typical stress-strain curves of specimens with varied crosslinker concentrations are shown in Figure S6. The hydrogels with lower MBAA

concentration (0.25 mol%) exhibited a higher tensile strain, while the tensile strengths of specimens at 0.5 mol% and 0.75 mol% MBAA concentrations are comparable and ~12.5% higher than specimens at MBAA concentration of 0.25 mol%. The increase in strength was due to the increased crosslinking density resulted from higher crosslinker concentrations, thus creating adequate three-dimensional crosslinking polymer structures. The obtained Young's modulus of specimens with 0.75 mol% MBAA concentration was ~10 MPa higher than 0.5 mol% and 0.25 mol%. However, hydrogel specimens with 0.25 mol% MBAA concentration yielded a higher toughness (~1.7 MJ m⁻³), about 15% and 17% increase from 0.5 mol% and 0.75 mol%, respectively. By tuning the MBAA concentrations, the printed hydrogels can have either superior tensile strength or improved toughness. Specifically, hydrogel specimens with 0.25 mol% MBAA concentration, which showed improved toughness and well-balanced hydrophilic and hydrophobic chain fractions, have comparable properties to load-bearing tissues like meniscus. The level of significance of the comparison between the tested specimens with different crosslinker concentrations were compared and the results were presented in Table S10-S12.

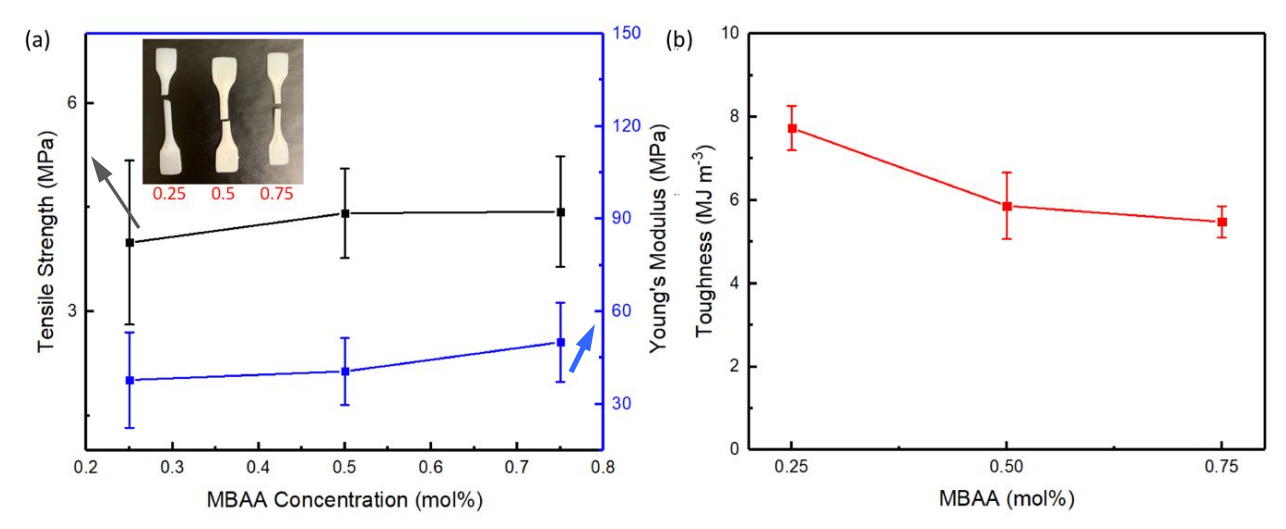


Figure 6. (a) Tensile strength and Young's modulus versus MBAA concentration; (b) Toughness versus MBAA concentration.

3.3 Compression characterization

Compression performance is critical to hydrogels for load-bearing tissue applications. Compression tests of hydrogel specimens with a series of PA:AAm concentrations were conducted. Figure 7a shows the typical compression stress-strain curves of P(PA-co-AAm)_(3.2) gels before and after solvent exchange. The organogel exhibited a higher compression strain (up to 70%) compared to the hydrogel specimen (less than 50%) with the same composition. However, the compression strength of hydrogel was ~21 MPa, about 13-fold higher than the organogel (~1.5 MPa). The compression strength and compressive modulus of varied PA:AAm concentrations are given in Figures 7b and 7c. At the same AAm concentration, the compression strength and compressive modulus increased with the increasing PA concentration due to the intrinsic rigidity of the benzene ring and enhanced benzene-benzene aggregation⁴¹. The compression strength and compressive moduli were ~31.1 MPa and ~65.5 MPa, respectively, for $P(PA-co-AAm)_{(4\cdot2)}$, ~9 MPa and ~20 MPa increased compared to $P(PA-co-AAm)_{(3\cdot2)}$ specimens. Similarly, the compression strength and compressive modulus slightly increased with the increasing amount of AAm with the same level of PA concentration. The compression strength and compressive modulus were ~21.2 MPa and ~41.8 MPa for P(PA-co-AAm)_(3:2), and increased to ~23 MPa and ~45.8 MPa when AAm concentration increased to 3 mol% at the same PA concentration. The increase was less significant compared to PA because AAm with linear alkene structure is known to be less hard than aromatic PA, thus exhibited a smaller impact in improving compression strength compared to PA. Compared to the printed specimens, the compressive strength and compressive modulus of the molded specimens with the same PA:AAm molar ratio were ~1.5 MPa and ~12 MPa higher.

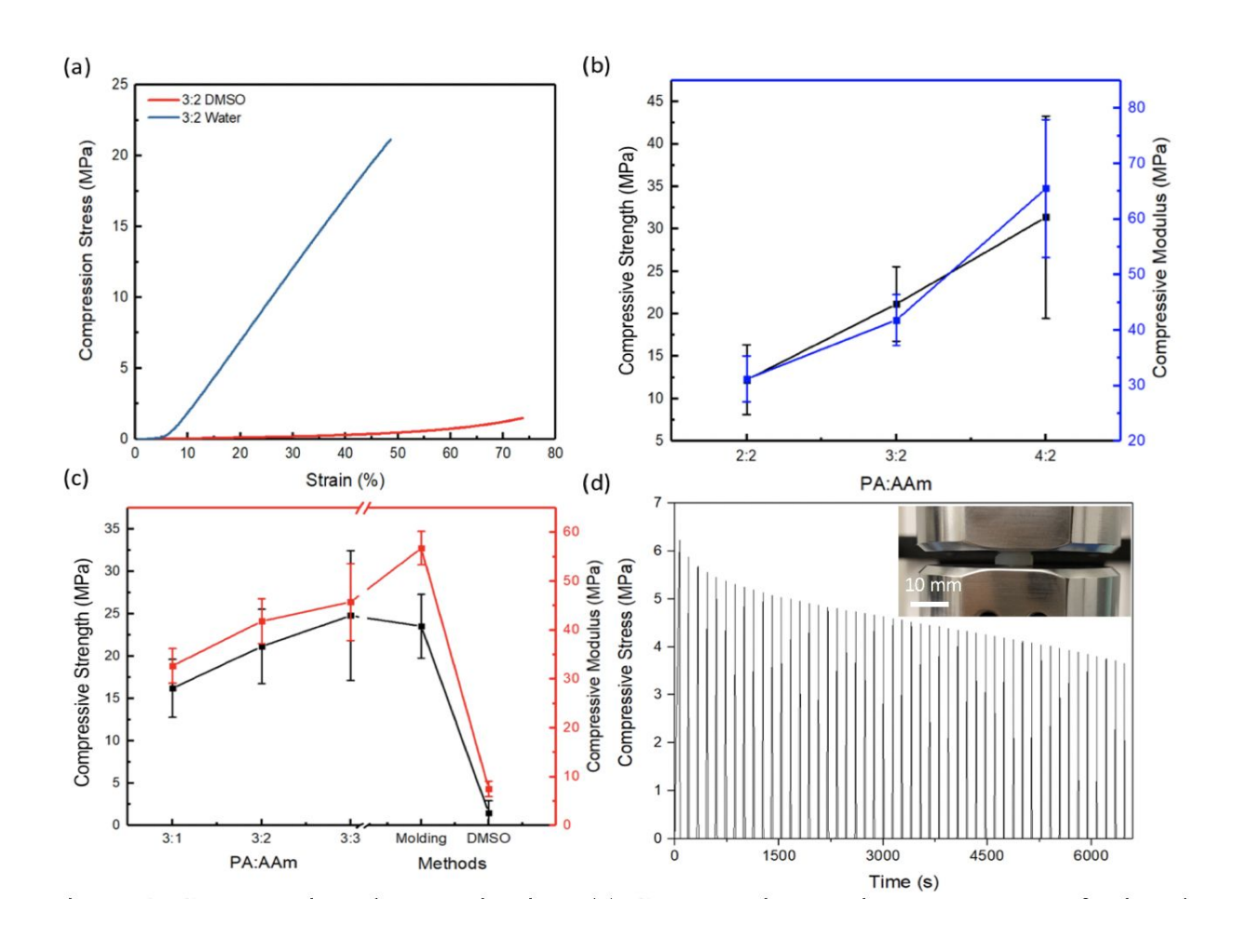


Figure 7. Compression characterization. (a) Compression strain-stress curve of printed hydrogel with PA:AAm composition of 3:2; (b) Compression strength as a function of AAm concentration and various treatment methods; (c) Compression strength as a function of PA concentration; (d) Dynamic compression test of 25 cycles.

To further test the dynamic performance of hydrogel under compression, a cylindrical hydrogel with P(PA-co-AAm)_(3:2) composition was compressed to a strain of 37% at a rate of 2 mm s⁻¹ and released to its original height at the same speed after holding the position for 1 s, as shown in the inset of Figure 7d. The specimens were continuously tested for 25 cycles. High levels of hysteresis are observed in the compression stress-strain curves of the first loading-

unloading cycle (Figure S7). After the first cycle, 34% of hysteresis was recovered in the second cycle. The deformation was not recoverable after waiting for 18 hours. This was due to the permanent damage of the PA region for further deformation while energy was only partially dissipated through soft AAm region. The maximum compression stress gradually decreased from ~6.18 MPa to 3.8 MPa after 25 compression iterations, as shown in Figure 7d. The previous damaged rigid region was softened and no longer effective in energy dissipation, which caused a decrease of maximum compression stress. All the characterized mechanical performance are summarized in Table 1.

Table 1. Mechanical properties of printed gel and bovine cartilage

Sample composition (PA:AAm)	Tensile strength (MPa)	Young's modulus (Tensile) (MPa)	Compressive strength (MPa)	Young's modulus (Compression) (MPa)	Toughness (kJ m ⁻³)
2:2 ^a	2.6 ± 0.35	27 ± 10.06	12.2 ± 4.11	31.2 ± 4.12	2.9 ± 0.88
3:2 ^a	4.4 ± 0.65	40.6 ± 10.83	21.2 ± 4.37	41.8 ± 4.59	5.9 ± 0.80
4:2 ^a	16.5 ± 3.94	232.4 ± 16.46	31.1 ± 11.94	65.5 ± 12.44	1.5 ± 0.86
3:1 ^a	0.4 ± 0.13	9.7 ± 6.18	16.2 ± 3.42	32.7 ± 3.54	0.1 ± 0.02
3:3 ^a	1.9 ± 0.26	5.2 ± 1.96	24 ± 7.64	45.8 ± 7.87	5.86 ± 0.80
Bovine Cartilage ²⁹	0.53-9	10.1-28.3	14-59	0.31	-

^a Contains with 0.5 wt% MBAA

3.4 Demonstration of 3D printing of meniscus

The capability of our printing process and proposed inks were tested. The demonstration of printing meniscus as a typical meniscus-like shape is given in Figure 8. Here, PA:AAm_(3:2) formulation was used for printing the artificial meniscus. Figure 8a shows the meniscus printing process using the extrusion-based bioprinter. The printed meniscus presented clear features, as shown in Figure 8b. The as-printed organogel was transparent and gradually became opaque white after immersing in DI water. After 60 min solvent exchange, the meniscus maintained the original features without noticeable shrinkage, as shown in Figure 8c. A 3D wide-area

measurement system (VR-5000 Series, Keyence) was used to further examine the precision of the printed artificial meniscus. The set up was shown in Figure S8. The printed meniscus (after 60 min solvent exchange) was positioned on the stage and scanned using the 3D measurement system, as shown in Figure S9. The original computer aided design (CAD) model and the generated model of 3D printed meniscus from 3D scanning were shown in Figure 8d and e, respectively. In addition, the top view of the original CAD model, the printed model and the overlay between the aforementioned two models were shown in Figure S9a, b, c, respectively. The inset in Figure S9b indicates the overall x-, y-dimension of the printed meniscus. In Figure S9c, the two models highly overlapped, and only observed a slight shrinkage in the printed model. A more detailed comparison of two models in height and position alignment was shown in Figure S10. The yellow and light blue represent the original CAD model and printed model, respectively. Only a ~0.4mm left-shift of the printed model was observed for the bottom area. The 3D height model was also generated by comparing the printed model to the original ones, as shown in Figure 8f. The height color bar was shown in the left of Figure 8f which indicated that the height difference between the two models were within the range of 1.5 mm. Specifically, green indicates zero difference in height, yellow and light blue indicate a slight (± 0.5 mm) difference and red and dark blue indicate a larger difference (± 1.5 mm). A more thorough comparison in height was shown in Figure S11.

The above demonstration is appealing. It suggested the feasibility of adopting 3D printing in patient-specific load-bearing tissue engineering. This will help in resolving current challenges in engineered meniscus fabrication²⁸.

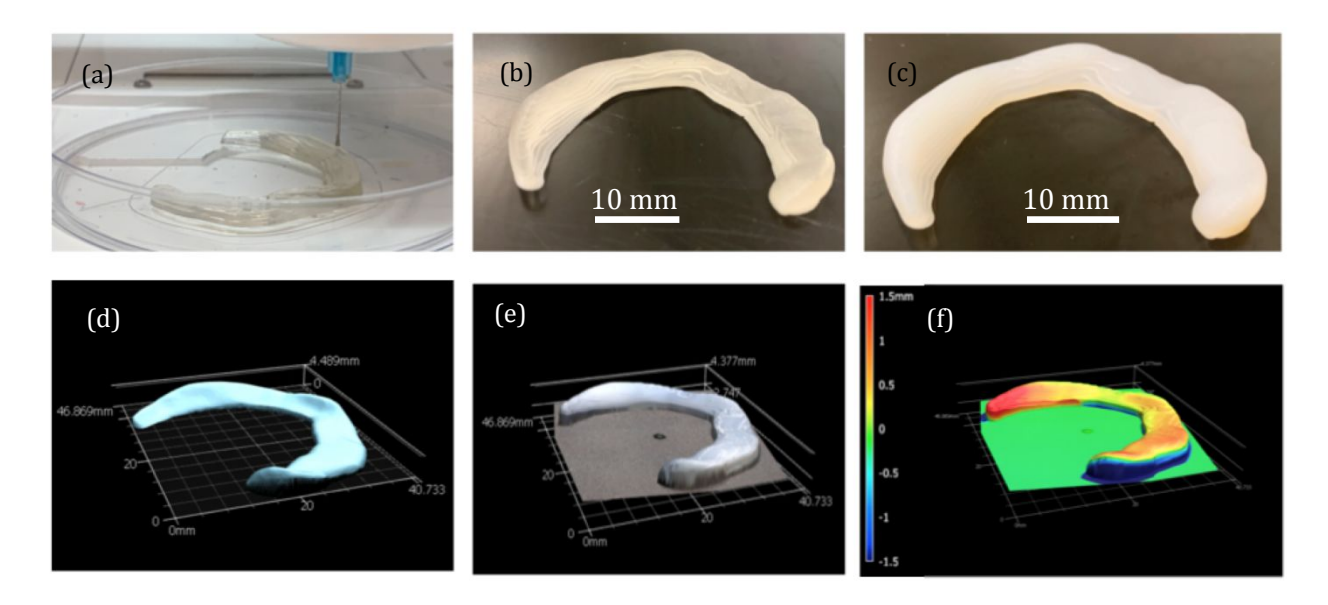


Figure 8. 3D printing of meniscus demonstration. (a) Printing process; (b) As-printed meniscus; (c) Obtained meniscus hydrogel after solvent exchange; (d) original CAD model; (e) printed model (60 min solvent exchange) generated from 3D scanning; (f) comparison of the original CAD model and printed model in height.

3.5 Comparison of 3D printed and molded hard hydrogels

PAAm has been known as one of the most promising hydrogels and used in many DN hydrogels as either soft or hard polymer network. A great number of PAAm based hydrogels accompany with other hard or soft, synthetic or natural biomaterials were reported^{11, 18, 28-30, 32, 42} and their results are summarized in Figure 9 and Table S14. In this work, instead of incorporating the PAAm polymer chain as one network, PAAm was introduced as one component in the alternated copolymer network of AAm and PA monomers. Figure 9 compares the mechanical properties (tensile strength and toughness) of the proposed P(PA-co-AAm) hydrogel with previously reported PAAm based DN hydrogels. The proposed P(PA-co-AAm) hydrogel with hydrophobic/hydrophilic components reached a tensile strength almost 3-fold

higher than the 3D printed hydrogels. The obtained toughness of the proposed hydrogel is comparable to the molded PAAm based hydrogels. Moreover, there was a big difference in 3D printed and molded structures due to the weak interlayer bonding. With the incorporation of the solvent exchange process, the interlayer bonding was strengthened.

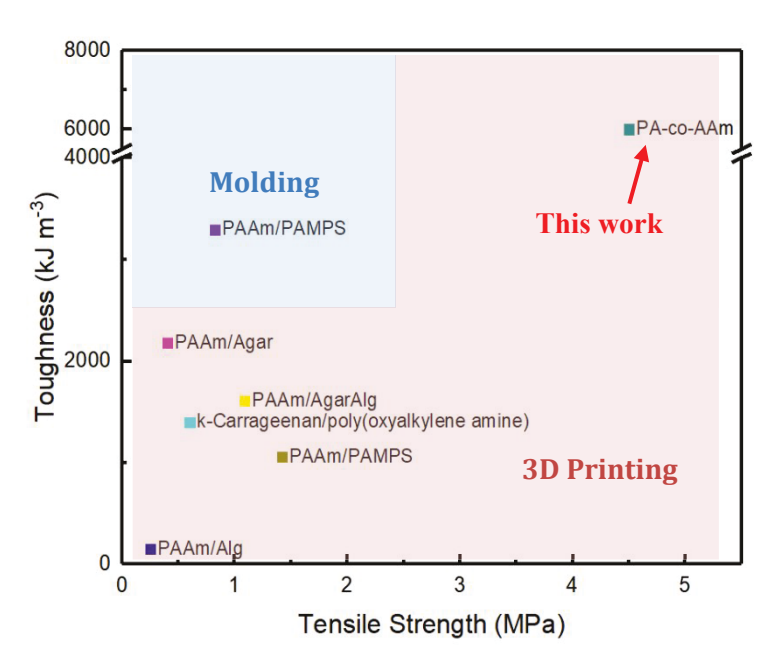


Figure 9. Comparison of tensile strength and toughness of PAAm based single polymer hydrogels^{15, 22, 28-29, 42-45}. The proposed hydrogel outperforms other 3D printed hydrogels. Compared with molded hydrogels, the proposed hydrogel has higher tensile strength and comparable work of extension.

Though the proposed copolymer structure with the designed alternating hard and soft region performed exceptional mechanical performance including strength and toughness, the introduction of benzene groups induced the poor anti-fatigue properties of the proposed gel. The future endeavor will focus on improving anti-fatigue properties of the proposed material, thus making it more suitable for artificial load-bearing tissues. Besides, the biocompatibility of the proposed gel remains unknown, the future work will examine the biological response to the

material and the fabricated artificial tissue. Both the in vivo and in vitro experiments will be conducted analyzing the toxicity and biocompatibility.

4. Conclusion

In conclusion, this research demonstrated a facile approach to 3D print a PA:AAm based single network copolymer hydrogel. The synergistic effect of the hydrophobic (PA) and hydrophilic (AAm) components induced a significant increase in tensile strength (~4.4 MPa), compressive strength (~20 MPa) and toughness (~6000 kJ m⁻³). The results are superior to a great number of 3D printed hydrogels. The hydrogel performance can be further improved by regulating the periodicity of the hydrophobic and hydrophilic region in the copolymers in the printing process. More importantly, this method can be extended to other high-performance copolymers to construct super strong hydrogels and thus pave the way to future 3D printing of load-bearing tissues like meniscus.

Acknowledgements

This work was supported by startup funds of Texas A&M University and Engineer Experimental Station (TEES), National Science Foundation (CMMI-1634858) and Water initiative grant which are gratefully appreciated.

ASSOCIATED CONTENT Supporting Information Available: FT-IR, SEM, and Rheological test, mechanical test details and geometric scanning analysis.

References

- 1. Kamata, H.; Akagi, Y.; Kayasuga-Kariya, Y.; Chung, U.; Sakai, T., "Nonswellable" Hydrogel Without Mechanical Hysteresis. *Science* **2014**, *343* (6173), 873-875.
- 2. Cao, L. X.; Shi, X. Y.; Chang, H. S.; Zhang, Q. F.; He, Y. N., pH-dependent recognition of apoptotic and necrotic cells by the human dendritic cell receptor DEC205. *Proceedings of the National Academy of Sciences of the United States of America* **2015**, *112* (23), 7237-7242.
- 3. Timothy Brindle, J. N., Darren L. Johnson, The Meniscus: Review of Basic Principles With Application to Surgery and Rehabilitation. *Journal of Athletic Training* **2001**, *36* (2), 10.

- 4. Rose, S.; Prevoteau, A.; Elziere, P.; Hourdet, D.; Marcellan, A.; Leibler, L., Nanoparticle solutions as adhesives for gels and biological tissues. *Nature* **2014**, *505* (7483), 382-+.
- 5. Sandring, S., Gray's Anatomy: The anatomical basis of clinical practice. *Elsevier Churchil Livingstone* **2009**, 5.
- 6. Packer, J. D.; Rodeo, S. A., Meniscal Allograft Transplantation. *Clinics in Sports Medicine* **2009**, *28* (2), 259-+.
- 7. A. J. Schoenfeld, W. J. L., D. B. Kay, Tissue-engineered meniscal constructs. *American Journal of Orthopedics* **2007**, *36* (11), 7.
- 8. Freeman, M. E.; Furey, M. J.; Love, B. J.; Hampton, J. M., Friction, wear, and lubrication of hydrogels as synthetic articular cartilage. *Wear* **2000**, *241* (2), 129-135.
- 9. Zhang, Z.; Wu, Q.; Zeng, L.; Wang, S. In *Modeling-Based Assessment of 3D Printing-Enabled Meniscus Transplantation*, 2019; Multidisciplinary Digital Publishing Institute: p 69.
- 10. Du, X.; Fu, S.; Zhu, Y., 3D printing of ceramic-based scaffolds for bone tissue engineering: an overview. *Journal of Materials Chemistry B* **2018**, *6* (27), 4397-4412.
- 11. Zhang, Z.; Wang, B.; Hui, D.; Qiu, J.; Wang, S., 3D bioprinting of soft materials-based regenerative vascular structures and tissues. *Composites Part B: Engineering* **2017**, *123*, 279-291.
- 12. Bilgen, B.; Jayasuriya, C. T.; Owens, B. D., Current Concepts in Meniscus Tissue Engineering and Repair. *Adv Healthc Mater* **2018**, *7* (11), e1701407.
- 13. Zhang, Y. S.; Khademhosseini, A., Advances in engineering hydrogels. *Science* **2017**, *356* (6337).
- 14. Fung, Y. C.; Liu, S. Q.; Zhou, J. B., Remodeling of the constitutive equation while a blood vessel remodels itself under stress. *Journal of biomechanical engineering* **1993**, *115* (4B), 453-459.
- 15. Gao, G.; Du, G.; Cheng, Y.; Fu, J., Tough nanocomposite double network hydrogels reinforced with clay nanorods through covalent bonding and reversible chain adsorption. *Journal of Materials Chemistry B* **2014**, *2* (11), 1539-1548.
- 16. Liu, R.; Liang, S.; Tang, X.-Z.; Yan, D.; Li, X.; Yu, Z.-Z., Tough and highly stretchable graphene oxide/polyacrylamide nanocomposite hydrogels. *Journal of Materials Chemistry* **2012**, *22* (28), 14160-14167.
- 17. Miyazaki, S.; Endo, H.; Karino, T.; Haraguchi, K.; Shibayama, M., Gelation mechanism of poly (N-isopropylacrylamide)—clay nanocomposite gels. *Macromolecules* **2007**, *40* (12), 4287-4295.
- 18. Chimene, D.; Peak, C. W.; Gentry, J. L.; Carrow, J. K.; Cross, L. M.; Mondragon, E.; Cardoso, G. B.; Kaunas, R.; Gaharwar, A. K., Nanoengineered Ionic-Covalent Entanglement (NICE) Bioinks for 3D Bioprinting. *ACS Appl Mater Interfaces* **2018**, *10* (12), 9957-9968.
- 19. Bakarich, S. E.; Beirne, S.; Wallace, G. G.; Spinks, G. M., Extrusion printing of ionic–covalent entanglement hydrogels with high toughness. *Journal of Materials Chemistry B* **2013**, *I* (38), 4939-4946.
- 20. Okumura, Y.; Ito, K., The polyrotaxane gel: A topological gel by figure of eight cross links. *Advanced materials* **2001**, *13* (7), 485-487.
- 21. Fleury, G.; Schlatter, G.; Brochon, C.; Hadziioannou, G., From high molecular weight precursor polyrotaxanes to supramolecular sliding networks. The 'sliding gels'. *Polymer* **2005**, *46* (19), 8494-8501.
- 22. Chen, Q.; Zhu, L.; Zhao, C.; Wang, Q.; Zheng, J., A robust, one pot synthesis of highly mechanical and recoverable double network hydrogels using thermoreversible sol gel polysaccharide. *Advanced materials* **2013**, *25* (30), 4171-4176.
- 23. Gong, J. P.; Katsuyama, Y.; Kurokawa, T.; Osada, Y., Double network hydrogels with extremely high mechanical strength. *Advanced Materials* **2003**, *15* (14), 1155-1158.
- 24. Sun, J. Y.; Zhao, X.; Illeperuma, W. R.; Chaudhuri, O.; Oh, K. H.; Mooney, D. J.; Vlassak, J. J.; Suo, Z., Highly stretchable and tough hydrogels. *Nature* **2012**, *489* (7414), 133-6.
- 25. Haque, M. A.; Kurokawa, T.; Gong, J. P., Super tough double network hydrogels and their application as biomaterials. *Polymer* **2012**, *53* (9), 1805-1822.
- 26. Chen, Q.; Chen, H.; Zhu, L.; Zheng, J., Fundamentals of double network hydrogels. *Journal of Materials Chemistry B* **2015**, *3* (18), 3654-3676.

- 27. Zhang, Z.; Jin, Y.; Yin, J.; Xu, C.; Xiong, R.; Christensen, K.; Ringeisen, B. R.; Chrisey, D. B.; Huang, Y., Evaluation of bioink printability for bioprinting applications. *Applied Physics Reviews* **2018**, *5* (4).
- 28. Yang, F.; Tadepalli, V.; Wiley, B. J., 3D Printing of a Double Network Hydrogel with a Compression Strength and Elastic Modulus Greater than those of Cartilage. *ACS Biomaterials Science & Engineering* **2017,** *3* (5), 863-869.
- 29. Wei, J.; Wang, J.; Su, S.; Wang, S.; Qiu, J.; Zhang, Z.; Christopher, G.; Ning, F.; Cong, W., 3D printing of an extremely tough hydrogel. *RSC Advances* **2015**, *5* (99), 81324-81329.
- 30. Li, X.; Wang, H.; Li, D.; Long, S.; Zhang, G.; Wu, Z., Dual Ionically Cross-linked Double-Network Hydrogels with High Strength, Toughness, Swelling Resistance, and Improved 3D Printing Processability. *ACS Appl Mater Interfaces* **2018**, *10* (37), 31198-31207.
- 31. Mredha, M. T. I.; Pathak, S. K.; Tran, V. T.; Cui, J.; Jeon, I., Hydrogels with Superior Mechanical Properties from the Synergistic Effect in Hydrophobic–Hydrophilic Copolymers. *Chemical Engineering Journal* **2018**.
- 32. Li, H.; Tan, Y. J.; Leong, K. F.; Li, L., 3D Bioprinting of Highly Thixotropic Alginate/Methylcellulose Hydrogel with Strong Interface Bonding. *ACS Appl Mater Interfaces* **2017**, *9* (23), 20086-20097.
- 33. Palaganas, N. B.; Mangadlao, J. D.; de Leon, A. C. C.; Palaganas, J. O.; Pangilinan, K. D.; Lee, Y. J.; Advincula, R. C., 3D Printing of Photocurable Cellulose Nanocrystal Composite for Fabrication of Complex Architectures via Stereolithography. *ACS Appl Mater Interfaces* **2017**, *9* (39), 34314-34324.
- 34. Siqueira, G.; Kokkinis, D.; Libanori, R.; Hausmann, M. K.; Gladman, A. S.; Neels, A.; Tingaut, P.; Zimmermann, T.; Lewis, J. A.; Studart, A. R., Cellulose Nanocrystal Inks for 3D Printing of Textured Cellular Architectures. *Advanced Functional Materials* **2017**, *27* (12).
- 35. Wang, J.; Chiappone, A.; Roppolo, I.; Shao, F.; Fantino, E.; Lorusso, M.; Rentsch, D.; Dietliker, K.; Pirri, C. F.; Grützmacher, H., All in One Cellulose Nanocrystals for 3D Printing of Nanocomposite Hydrogels. *Angewandte Chemie International Edition* **2018**, *57* (9), 2353-2356.
- 36. Wang, Q.; Sun, J.; Yao, Q.; Ji, C.; Liu, J.; Zhu, Q., 3D printing with cellulose materials. *Cellulose* **2018**, *25* (8), 4275-4301.
- 37. Mezger, T. G., *The rheology handbook: for users of rotational and oscillatory rheometers.* Vincentz Network GmbH & Co KG: 2006.
- 38. Darby, R.; Darby, R.; Chhabra, R. P., *Chemical engineering fluid mechanics, revised and expanded*. CRC Press: 2001.
- 39. Arimoto, H.; Egawa, M., Imaging wavelength and light penetration depth for water content distribution measurement of skin. *Skin Research and Technology* **2015**, *21* (1), 94-100.
- 40. Bhosale, A. M.; Richardson, J. B., Articular cartilage: structure, injuries and review of management. *British medical bulletin* **2008**, *87* (1), 77-95.
- 41. Iwasaki, T.; Kohinata, Y.; Nishide, H., Poly (thiaheterohelicene): a stiff conjugated helical polymer comprised of fused benzothiophene rings. *Organic letters* **2005**, *7* (5), 755-758.
- 42. Bakarich, S. E.; Panhuis, M. i. h.; Beirne, S.; Wallace, G. G.; Spinks, G. M., Extrusion printing of ionic-covalent entanglement hydrogels with high toughness. *Journal of Materials Chemistry B* **2013**, *1* (38).
- 43. Bakarich, S. E.; Balding, P.; Gorkin Iii, R.; Spinks, G. M., Printed ionic-covalent entanglement hydrogels from carrageenan and an epoxy amine. *RSC Advances* **2014**, *4* (72), 38088-38092.
- 44. Liang, J.; Shan, G.; Pan, P., Double network hydrogels with highly enhanced toughness based on a modified first network. *Soft Matter* **2017**, *13* (22), 4148-4158.
- 45. Gong, J. P., Why are double network hydrogels so tough? *Soft Matter* **2010**, *6* (12).

Table of Contents graphic:

